MATHEMATICAL BIOSCIENCES

ISSN: 0025-5564

ELSEVIER

(Accepted November 29th 2016

ELECTRO-KINETICALLY DRIVEN PERISTALTIC TRANSPORT OF VISCOELASTIC PHYSIOLOGICAL FLUIDS THROUGH A FINITE LENGTH CAPILLARY: *MATHEMATICAL MODELLING*

***[1]Dharmendra Tripathi, [1]Ashu Yadav** and **[2]O. Anwar Bég**

[1]Department of Mechanical Engineering, Manipal University, Jaipur-303007, India.
[2] Fluid Dynamics, Bio-Propulsion and Nanosystems, Department of Mechanical and Aeronautical Engineering, Salford University, Newton Building, The Crescent, Salford, M54WT, England, UK.
*******Corresponding author- email: dharmtri@gmail.com*

ABSTRACT

Analytical solutions are developed for the electro-kinetic flow of a viscoelastic biological liquid in a finite length cylindrical capillary geometry under peristaltic waves. The Jefferys' non-Newtonian constitutive model is employed to characterize rheological properties of the fluid. The unsteady conservation equations for mass and momentum with electro-kinetic and Darcian porous medium drag force terms are reduced to a system of steady linearized conservation equations in an axisymmetric coordinate system. The long wavelength, creeping (low Reynolds number) and Debye–Hückel linearization approximations are utilized. The resulting boundary value problem is shown to be controlled by a number of parameters including the electro-osmotic parameter, Helmholtz-Smoluchowski velocity (maximum electro-osmotic velocity), and Jefferys' first parameter (ratio of relaxation and retardation time), wave amplitude. The influence of these parameters and also time on axial velocity, pressure difference, maximum volumetric flow rate and streamline distributions (for elucidating trapping phenomena) is visualized graphically and interpreted in detail. Pressure difference magnitudes are enhanced consistently with both increasing electro-osmotic parameter and Helmholtz-Smoluchowski velocity, whereas they are only elevated with increasing Jefferys' first parameter for positive volumetric flow rates. Maximum time averaged flow rate is enhanced with increasing electro-osmotic parameter, Helmholtz-Smoluchowski velocity and Jefferys' first parameter. Axial flow is accelerated in the core (plug) region of the conduit with greater values of electro-osmotic parameter and Helmholtz-Smoluchowski velocity whereas it is significantly decelerated with increasing Jefferys' first parameter. The simulations find applications in electro-osmotic (EO) transport processes in capillary physiology and also bio-inspired EO pump devices in chemical and aerospace engineering.

Keywords: *Electro-osmosis; Peristalsis; Finite* Debye length*; Jeffrey Fluids; Relaxation time; microfluidics.*

1. INTRODUCTION

The study of electro-kinetics in biological and bio-inspired systems is attaining considerable importance owing to its applications in bio-micro-electro-mechanical-systems (bioMEMS), microfluidics-based biomedical separation, bio-chip systems for drug delivery and biomedical diagnostics [1-3]. Electro-kinetics is the study of fluid flow generated by the imposition of an external electric field in an electrolyte-filled conduit with electric double layers on its wetted surfaces. Owing to the continuous miniaturization of many industrial, biomedical and other systems, the influence of electrical forces is greatly increased in micro-channel transport processes. This has mobilized significant scientific interest in simulating the complex fluid dynamical features of such processes aimed at optimizing performance in real applications, including medicine. In recent years therefore many researchers have formulated various electro-kinetic fluid dynamics models (both laminar and turbulent) to predict the interplay between electrical, viscous and other body forces and geometric features. Kang *et al*. [4] studied the electroosmotic flow in a cylindrical microcapillary and found the solution of Poisson–Boltzmann equation for arbitrary zeta-potentials. A similar study was reported in [5] in which electroosmotic flow was analysed through an annulus under the situation when both concentric cylindrical walls carry high zeta potentials. Devasenathipathy and Santiago [6] studied the electrokinetic flow diagnostics using micro- and nano-scale diagnostic techniques. Minerick *et al.* [7] experimentally examined the electrokinetic flow of a suspension of erythrocytes (red blood cells, RBCs) in 20 micron cylindrical fused-silica capillaries. Chung *et al*. [8] presented low power and robust electroactive microwell-based implantable drug delivery system, intended for use with autonomous microsystems. A diverse spectrum of theoretical models of electroosmotic fluid mechanics are presented in [9-11]. Recently Mohammadi *et al*. [12] designed a microfluidic device combining hydrodynamic and dielectrophoretic techniques to separate plasma from fresh blood in a microfluidic channel. This study achieved for the first time a robust methodology for optical real-time monitoring of the components of plasma without pre- or post-processing. Sinha and Shit [13] presented a mathematical model for blood flow through capillary by considering electromagnetic body forces in addition to convection heat transfer effects. They considered the case where the height of the capillary significantly exceeds the thickness of electrical double layer comprising the stern and diffuse layers and noted that blood temperature may be regulated effectively with Ohmic magnetic dissipation (Joule heating) parameter.

In the above investigations, electrokinetic effects on fluid flow with biological applications have been presented and some microfluidics devices have been engineered exploiting this principle. However, in these systems the boundaries have invariably been *rigid* i.e. non-flexible. Peristaltic flow is a mechanism for transportation of physiological fluids by rhythmic muscle contraction followed by relaxation and is a highly efficient, adaptive, intelligent and sustainable methodology for propulsion in flexible-walled conduits [14]. It exemplifies biological compromise between strength and compliance which enables many medical and zoological systems to function with stunning efficiency. It arises in human and animal physiological phenomena and pertinent examples include uro-dynamic transport from the kidneys to the bladder, chyme dynamics in the gastrointestinal tract, vaso-motion in small blood vessels, swallowing of food through the oesophagus, ovum transport in the female fallopian tube, and lymph movement in the lymphatic vessels and transport of spermatozoa in the ductus efferents of the male reproductive tract. An excellent perspective of these applications is provided by Fung [15]. Furthermore peristaltic transport is fundamental to the versatile locomotion of certain earthworms (Lumbricus terrestris) [16, 17], phloem trans-location in botanical systems (trees, plants) [18, 19] and respiratory pentasome functioning in reptiles [20]. Many modern devices have implemented peristaltic mechanisms including heart lung machines, dialysis machines, blood pump machines, and roller pumps.

In parallel with progress in laboratory fabrication of systems, many mathematical and computational investigations of peristaltic flow have also been communicated. A very interesting and influential theoretical model on peristaltic flow under low Reynolds number and long wavelength has been presented by Shapiro *et al.* [20] in which reflux and trapping phenomena are discussed in detail. Most studies in the literature are however constrained to steady flow and infinite conduits. The vast majority of physiological flows are by nature, *unsteady* and propagate in *finite length* conduits. The formulation in [21] has therefore been improved by a number of researchers for unsteady peristaltic flows in finite length tubes. An excellent example is the study of Li and Brasseur [22] who considered both single and multiple train wave propagation. Brasseur and Dodds [23] described numerical results which concur well with the manometer observation for swallowing of a single food bolus. These studies while physically more realistic than earlier analyses, have nevertheless been confined to the *Newtonian* i.e. Navier-Stokes model. Many real working fluids in electro-osmotic devices and peristaltic propulsion mechanisms are strongly *non-Newtonian*. Viscoelasticity in particular has been confirmed to be a critical feature of numerous medical fluids, as elucidated by

Goldsmith [24] and de Vincente [25]. Biopolymeric solutions and gels deployed in biomedical devices are also frequently strongly viscoelastic in nature [26]. Non-Newtonian (rheological) peristaltic flow simulation has evolved into a significant area of modern biological fluid dynamics. Many simple and more sophisticated constitutive equations have been employed to improve the accuracy of mathematical models, which provide an important compliment to clinical studies. These rheological models capture different characteristics of real liquids including shear thinning, thixotropy, relaxation, retardation, memory, couple stresses, micro-continuum features, stretch and swelling, all of which arise in physiology. Chaube *et al.* [27] considered peristaltic slip flow of Ostwald-DeWaele power law in tapered conduits. Ali *et al.* [28] derived perturbation solutions for third grade differential viscoelastic fluids in peristaltic pumping through curved channels. Tripathi and Bég [29] studied peristaltic pumping of fractional second order Reiner-Rivlin viscoelastic fluids with Froude number effects. Kiran *et al*. [30] simulated chemical reaction and Taylor dispersion effects in peristaltic pumping of Eringen micropolar fluids in an attempt to characterize the physico-chemical features of gastric breakdown. Further studies have employed Stokes couple stress (polar) fluids [31] and elasto-viscous Williamson nanofluids [32]. A particularly elegant non-Newtonian viscoelastic model, is the Jefferys viscoelastic model which features both retardation and relaxation effects. It employs a convective derivative instead of the customary time derivative encountered in other viscoelastic models. This model has proved extremely popular and versatile and has been implemented in many diverse problems in biomedical flows including pulsed Couette flows (using Lattice Boltzmann methods) [33] and biopolymeric thermal enrobing flows [34] using Keller box finite difference methods. Khadrawi *et al.* [35] investigated fundamental biophysical engineering flows using the Jefferys model including transient Couette flow and transient Poiseuille flow in a channel. They derived closed-form solutions and noted that with increasing dimensionless relaxation time the flow response to the imposed driving force is markedly slower, implying that the fluid requires a greater time to absorb the effect of a driving force and therefore there is an associated delay in achieving steady-state behaviour. Akbar *et al*. [36] studied Jefferys non-Newtonian blood flow through a tapered artery with a stenosis deriving perturbation solutions for velocity, wall shear stress, shearing stress at the stenosis throat, and impedance of the artery. Several works relating to peristaltic pumping of Jefferys viscoelastic fluids have also been presented. Alarabi *et al.* [37] applied He's powerful homotopy perturbation method (HPM) to investigate variable viscosity effects in peristaltic pumping and heat transfer of Jeffreys viscoelastic fluid in an eccentric cylindrical annulus, as a simulation of endoscopy. Tripathi *et al*. [38] derived analytical solutions for thermal

convection effects on esophageal transport of viscoelastic materials. They observed that pressure along the entire length of the food pipe geometry (channel) reduces with greater relaxation time (fixed retardation time) whereas it is enhanced by increasing the magnitude of retardation time (fixed relaxation time).

Motivated from the wide applications of electro-kinetic effects in biomedical engineering, in the present article, we present a theoretical study on peristaltic transport driven by electroosmotic means in Jefferys viscoelastic fluids. The objective is double fold. *Firstly* we extend the work of Chakraborty [39] which was limited to thin electric double layer (EDL) i.e. electroosmotic slip boundary condition is taken in account and external electric field effects are neglected. *Secondly* we provide a new non-Newtonian formulation to extend the existing studies in rheological electro-osmotic transport. Previous works have considered power-law fluids [40], simplified Phan-Thien–Tanner viscoelastic fluids [41] and viscoplastic (Casson, Herschel-Bulkley, and Bingham fluids) [42]. Important aspects in electro-osmotic peristaltic rheological propulsion require further elucidation. Paramount among these are the need to elaborate in more detail how external electric field controls the peristaltic flow and how the Debye length (characteristic thickness of the electrical double layer i.e. EDL) improves peristaltic pumping. It is also of great interest to clarify with more precision the impact of oscillating flow on electrical potential profiles. This paper therefore studies the *electro-kinetic effects on peristaltic transport of a Jefferys viscoelastic electrolyte through a finite length tube*. The effects of Debye length and Helmholtz-Smoluchowski velocity on peristaltic pumping and trapping are evaluated analytically and explored further with the aid of graphical visualization using Mathematica software. The finite length tube Newtonian model Li and Brasseur [22] is shown to be a special case of the present study. The current computations are relevant to physiological electro-osmotic processes e.g. cylindrical electrophoresis cells [43, 44] and also bio-inspired electro-chemical pumps [45].

2. MATHEMATICAL MODEL

The geometric model for the electro-osmotic peristaltic transport through a finite length (L) cylindrical tube, as depicted in **Fig.1,** is mathematically considered as:

$$\bar{h}(\bar{x},\bar{t}) = a - \bar{\phi}\cos^2\frac{\pi}{\lambda}(\bar{x} - c\bar{t}) \quad \forall\, x \in [0,\, L], \tag{1}$$

where $\underline{\bar{h}}$, $\bar{x}$, $\bar{t}$, a , $\bar{\phi}$, λ , c , L are the radial displacement of the wall surface, axial coordinate, time, radius of tube, amplitude, wavelength, wave velocity, and tube length.

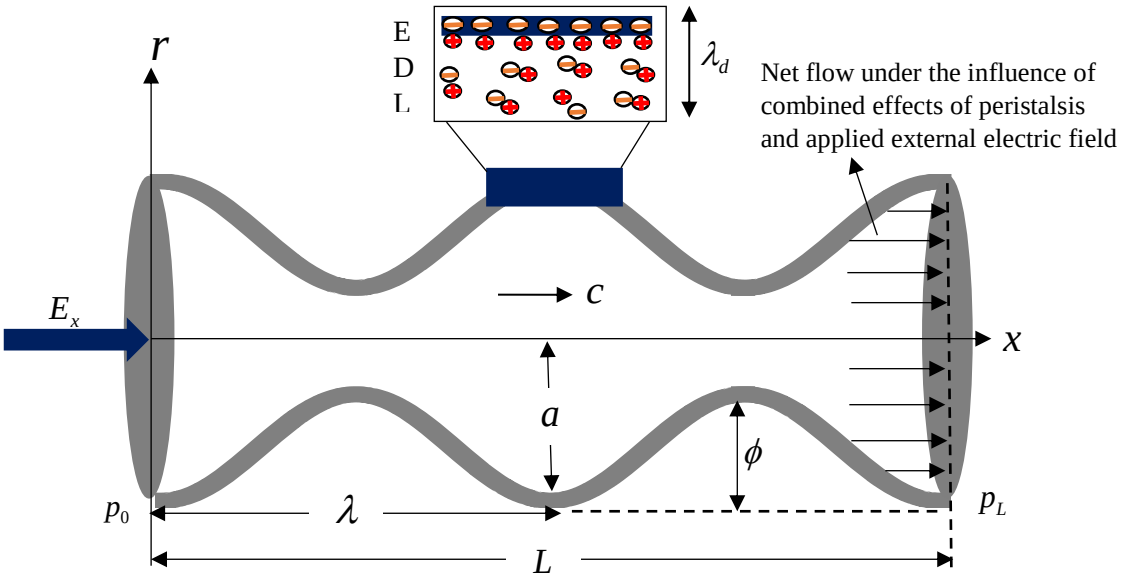

Fig.1. A geometrical description of flow regime altered by applied external electric field (E_x) through a finite length (L) circular capillary of radius (a) with travelling by peristaltic wave propagations with a wave velocity (c), wavelength (λ), and amplitude (ϕ). The pressures at the left and right reservoirs (inlet and exit, respectively) are denoted as p_0 and p_L respectively. The electric double layer (EDL) is also sketched to show the ions distribution with Debye length (λ_d).

Most solid surfaces tend to acquire a net surface charge (+ve or –ve) when brought into contact with an aqueous (polar) solvent. For a symmetric (*z*: *z*) binary electrolyte solution (Na^+ Cl^-), the electric potential distribution is developed due to the presence of electrical double layer (EDL) in the micro-channel, described by the Poisson-Boltzmann equation:

$$\nabla^2 \overline{\Phi} = -\frac{\overline{\rho}_e}{\varepsilon}, \tag{2}$$

in which, ∇^2 is Laplacian operator, $\overline{\Phi}$ is potential function, ρ_e is the density of the total ionic change, ε is the permittivity. For a symmetric (z:z) electrolyte, the density of the total ionic energy, ρ_e is given by, $\rho_e = ez(n^+ - n^-)$, in which z is charge balance, e is the electronic charge, n^+ and n^- are the number densities of cations and anions respectively and are given by Boltzmann distribution (considering no EDL overlap):

$$n^{\pm} = n_0 Exp\left[\pm \frac{e\, z\, \overline{\Phi}}{K_B T}\right], \tag{3}$$

where n_0 represents the concentration of ions at the bulk, which is independent of surface electro-chemistry, K_B is the Boltzmann constant, T is the average temperature of the electrolytic solution.

This distribution of ionic concentration appears to be valid when there is no axial gradient of the ionic concentration within the micro-channel and the flow Peclét number is assumed to be significantly small. Combining the Eqns. (2) & (3), we obtain the *Poisson-Boltzmann* equation in the form:

$$\frac{1}{\bar{r}}\frac{\partial}{\partial \bar{r}}\left(\bar{r}\frac{\partial \overline{\Phi}}{\partial \bar{r}}\right)=\frac{2n_0 ez\sinh\left(\frac{ez\overline{\Phi}}{K_B T}\right)}{\varepsilon}. \tag{4}$$

Introducing a normalized electro-osmotic potential function, $\overline{\Phi}$, with zeta potential ζ of the medium along with other non-dimensional variables, like $\Phi=\frac{\overline{\Phi}}{\zeta}$ and $r=\frac{\bar{r}}{a}$ (normalized radial coordinate) and using the Debye–Hückel linearization approximation $\sinh\left(\frac{ez\Phi}{K_B T}\right)\approx\frac{ez\Phi}{K_B T}$, Eqn.(4) reduces to:

$$\frac{1}{r}\frac{\partial}{\partial r}\left(r\frac{\partial \Phi}{\partial r}\right)=\kappa^2\Phi, \tag{5}$$

where $\kappa=aez\sqrt{\frac{2n_0}{\varepsilon K_B T}}=\frac{a}{\lambda_d}$, is known as the electro-osmotic parameter and $\lambda_d\propto\frac{1}{\kappa}$ is Debye length or characteristic thickness of electrical double layer (EDL). Using the boundary conditions: $\left.\frac{\partial\Phi}{\partial r}\right|_{r=0}=0$ and $\Phi|_{r=h}=1$, since the *potential function is symmetric*, the potential function is obtained as:

$$\Phi=\frac{I_0(\kappa r)}{I_0(\kappa h)}, \tag{6}$$

where $I_0(\kappa r)$ is modified Bessel function of first kind of zero order.

Under the above approximations, the fundamental equations for axisymmetric incompressible flow with an axially applied electrokinetic body force term taken into account are given as:

$$\frac{\partial \bar{u}}{\partial \bar{x}}+\frac{1}{\bar{r}}\frac{\partial(\bar{r}\bar{\mathrm{v}})}{\partial \bar{r}}=0, \tag{7}$$

$$\rho\left(\frac{\partial}{\partial \bar{t}}+\bar{u}\frac{\partial}{\partial \bar{x}}+\bar{\mathrm{v}}\frac{\partial}{\partial \bar{r}}\right)\bar{u}=-\frac{\partial \bar{p}}{\partial \bar{x}}+\frac{\partial \bar{S}_{\bar{x}\bar{x}}}{\partial \bar{x}}+\frac{1}{\bar{r}}\frac{\partial(\bar{r}\bar{S}_{\bar{x}\bar{r}})}{\partial \bar{r}}+\bar{\rho}_e E_x, \tag{8}$$

$$\rho\left(\frac{\partial}{\partial \bar{t}}+\bar{u}\frac{\partial}{\partial \bar{x}}+\bar{\mathrm{v}}\frac{\partial}{\partial \bar{r}}\right)\bar{\mathrm{v}}=-\frac{\partial \bar{p}}{\partial \bar{r}}+\frac{\partial \bar{S}_{\bar{r}\bar{x}}}{\partial \bar{x}}+\frac{1}{\bar{r}}\frac{\partial(\bar{r}\bar{S}_{\bar{r}\bar{r}})}{\partial \bar{r}}, \tag{9}$$

where $\bar{S}_{\bar{x}\bar{x}}, \bar{S}_{\bar{x}\bar{r}}, \bar{S}_{\bar{r}\bar{x}}, \bar{S}_{\bar{r}\bar{r}}$ are the extra stress components and $\rho, \bar{u}, \bar{\mathrm{v}}, \bar{p},$ and E_x denote the fluid density, axial velocity, radial velocity, pressure, and elctrokinetic body force. The constitutive equation of extra stress $\bar{S}$ for Jeffrey model, following [34]-[38] may be defined as:

$$\bar{S}=\frac{\mu}{1+\lambda_1}\{\dot{\gamma}+\lambda_2\ddot{\gamma}\}, \tag{10}$$

where $\mu, \dot{\gamma}, \lambda_1, \lambda_2$ are the dynamic viscosity, rate of strain, the ratio of relaxation and retardation time, the retardation time and dots denote differentiation with respect to time.

We then introduce the following non-dimensional parameters:

$$x=\frac{\bar{x}}{\lambda}, t=\frac{c\bar{t}}{\lambda}, u=\frac{\bar{u}}{c}, \mathrm{v}=\frac{\bar{\mathrm{v}}}{c\delta}, \delta=\frac{a}{\lambda}, h=\frac{\bar{h}}{a}, \quad \phi=\frac{\bar{\phi}}{a}, p=\frac{\bar{p}a^2}{\mu c\lambda}, \mathrm{Re}=\frac{\rho c a}{\mu}, \tag{11}$$

It is assumed that the wavelength of the pulse (peristaltic wave) is much larger than the channel height; i.e. we assume that the lubrication approximation is valid ($\delta = a/\lambda << 1$). The nonlinear terms in the momentum equation are found to be $O\left(Re\,\delta^2\right)$, Re being the Reynolds number (based on the peristaltic wave velocity and tube radius), δ denotes the ratio of the radial length scale to the axial length scale. On similar lines, the nonlinear terms in the Nernst Planck equations are $O\left(Pe\,\delta^2\right)$, where $Pe = Re\,Sc$ represents the ionic Peclet number and $Sc = \mu/\rho D$ denotes the Schmidt number. Therefore, the nonlinear terms may be dropped in the limit that ($Re, Pe, \delta << 1$). In this limit, the governing equations reduce to:

$$\frac{\partial u}{\partial x}+\frac{1}{r}\frac{\partial(r\mathrm{v})}{\partial r}=0, \tag{12}$$

$$\frac{\partial p}{\partial x}=\frac{1}{(1+\lambda_1)r}\frac{\partial}{\partial r}\left(r\frac{\partial u}{\partial r}\right)+\kappa^2 U_{HS}\frac{I_0(\kappa r)}{I_0(\kappa h)}, \tag{13}$$

$$\frac{\partial p}{\partial r} = 0. \tag{14}$$

where $U_{HS} = -\frac{E_x \varepsilon \zeta}{\mu c}$ is the Helmholtz-Smoluchowski velocity or *maximum* electro-osmotic velocity. The relevant boundary conditions following Li & Brasseur [**22**] are specified as follows:

$$\left.\frac{\partial u}{\partial r}\right|_{r=0} = 0, u\big|_{r=h} = 0, \mathrm{v}\big|_{r=0} = 0, \mathrm{v}\big|_{r=h} = \frac{\partial h}{\partial t}, p\big|_{x=0} = p_0, p\big|_{x=L} = p_L, \tag{15}$$

Using boundary conditions (15), the *axial velocity* solution of Eqn.(13) emerges as:

$$u = (1+\lambda_1)\left\{\frac{1}{4}\frac{\partial p}{\partial x}\left(r^2 - h^2\right) - U_{HS}\left(\frac{I_0(\kappa r)}{I_0(\kappa h)} - 1\right)\right\}. \tag{16}$$

Using the Eq.(16) and boundary condition (15), the *radial velocity* from the mass conservation (continuity) equation is obtained as:

$$\mathrm{v} = (1+\lambda_1)\left[\frac{r}{4}\left\{-\frac{\partial^2 p}{\partial x^2}\left(\frac{r^2}{4} - \frac{h^2}{2}\right) + h\frac{\partial p}{\partial x}\frac{\partial h}{\partial x}\right\} - U_{HS}\frac{I_1(\kappa r) I_1(\kappa h)}{(I_0(\kappa h))^2}\frac{\partial h}{\partial x}\right], \tag{17}$$

where $I_1(\kappa r)$ is the modified Bessel function of the first kind of first order.

Using Eq.(17) and boundary conditions (15), the *pressure gradient* is obtained as:

$$\frac{\partial p}{\partial x} = \frac{1}{h^4}\left[G_0(t) + 16\int_0^x \left\{\frac{h}{(1+\lambda_1)}\frac{\partial h}{\partial t} + U_{HS} h \frac{\partial h}{\partial s}\left(\frac{I_1(\kappa h)}{I_0(\kappa h)}\right)^2\right\} ds\right], \tag{18}$$

where $G_0(t)$ is arbitrary function of t to be evaluated by using finite length boundary conditions (15). The *pressure difference* can be computed *along the axial length* by

$$\Delta p = p(x,t) - p(0,t) = \int_0^x \frac{\partial p}{\partial s} ds, \tag{19}$$

and $G_0(t)$ is expressed as:

$$G_0(t)=\frac{(p_l-p_0)-16\int_0^L h^{-4}\int_0^x\left\{\frac{h}{(1+\lambda_1)}\frac{\partial h}{\partial t}+U_{HS}h\frac{\partial h}{\partial s}\left(\frac{I_1(\kappa h)}{I_0(\kappa h)}\right)^2\right\}dsdx}{\int_0^L h^{-4}dx}. \tag{20}$$

The *volumetric flow rate* in the fixed frame is defined as:

$$Q(x,t)=2\int_0^h urdr=(1+\lambda_1)\left\{-\frac{h^4}{8}\frac{\partial p}{\partial x}+U_{HS}\left(h^2-\frac{2hI_1(\kappa h)}{\kappa I_0(\kappa h)}\right)\right\}. \tag{21}$$

Rearranging the Eq.(21), the pressure gradient in the form of volumetric flow rate is expressed as:

$$\frac{\partial p}{\partial x}=\frac{8}{h^4}\left\{-\frac{Q(x,t)}{(1+\lambda_1)}+U_{HS}\left(h^2-\frac{2hI_1(\kappa h)}{\kappa I_0(\kappa h)}\right)\right\}. \tag{22}$$

The transformations in dimensional form between a wave frame (x_w, y_w) moving with velocity (c) and the fixed frame (x, y) are given by :

$$x=x_w-ct,\quad r=r_w,\quad u=u_w+c,\quad v=v_w, \tag{23}$$

where (u_w, v_w) and (u, v) are the velocity components in the wave and fixed frame respectively.

The *volumetric flow rate in the wave frame* is given by

$$q_w=2\int_0^h r_w u_w dr_w=2\int_0^h r(u-1)dr, \tag{24}$$

which, on integration, yields:

$$q_w=Q-h^2. \tag{25}$$

The pumping performance is characterized for periodic train waves by averaging the volumetric flow rate for one time interval i.e. a *time-averaged volume flow rate* is employed which, following Shapiro *et al*. [20], is defined as:

$$\bar{Q}=\int_0^1 Qdt=\int_0^1 (q_w+h^2)dt, \tag{26}$$

which, on integration, yields

$$\bar{Q} = \int_0^1 Q dt = Q - h^2 + 1 - \phi + 3\phi^2 / 8. \tag{27}$$

Using Eqs.(22) & (27), the pressure gradient in wave frame is expressed as:

$$\frac{\partial p}{\partial x_w} = \frac{8}{h^4}\left\{ -\frac{\bar{Q} + h^2 - 1 + \phi - 3\phi^2/8}{(1+\lambda_1)} + U_{HS}\left(h^2 - \frac{2hI_1(\kappa h)}{\kappa I_0(\kappa h)} \right) \right\}. \tag{28}$$

Integrating the Eq.(28) from 0 to 1, the pressure difference across one wavelength is obtained as:

$$\Delta p_1 = p(1) - p(0) = \int_0^1 \frac{8}{h^4}\left\{ -\frac{\bar{Q} + h^2 - 1 + \phi - 3\phi^2/8}{(1+\lambda_1)} + U_{HS}\left(h^2 - \frac{2hI_1(\kappa h)}{\kappa I_0(\kappa h)} \right) \right\} dx_w. \tag{29}$$

Using Eqn.(16), the *stream function* in the wave frame (obeying the Cauchy-Riemann equations, $u = \frac{1}{r}\frac{\partial \psi}{\partial r}$ and $v = -\frac{1}{r}\frac{\partial \psi}{\partial x}$) takes the form:

$$\psi = (1+\lambda_1)\left\{ \frac{1}{16}\frac{\partial p}{\partial x}(r^4 - 2r^2h^2) - U_{HS}\left(\frac{rI_1(\kappa r)}{\kappa I_0(\kappa h)} - \frac{r^2}{2} \right) \right\}. \tag{30}$$

All the above expressions will reduce to expressions of Li and Brasseur [22] for $U_{HS} = 0$ & $\lambda_1 = 0$ i.e. without external electrical field and viscoelastic properties. The above expressions will also reduce to expressions for peristaltic propulsion with thin EDL effects (i.e. only electroosmotic slip velocity at the wall is considered, neglecting external electric field effects) and correspond to the case examined by Chakraborty [39]) which is retrieved from the present general model for $\kappa \to \infty$ i.e. when the thickness of EDL tends to zero ($\lambda_d \to 0$).

3. NUMERICAL RESULTS AND DISCUSSION

Comprehensive numerical solutions have been obtained based on the analytical solutions derived in section 2, via Mathematica symbolic software. Simpson's 1/3 rule is employed to perform the numerical integration. These are presented in **Figs. 2-8**. We confined attention to discussing the effects of three parameters on the peristaltic pumping characteristics and trapping phenomenon, namely **1)** *electro-osmotic parameter* ($\kappa = aez\sqrt{\frac{2n_0}{\varepsilon K_B T}} = \frac{a}{\lambda_d}$), which inversely proportional to Debye length (λ_d) or characteristic thickness of electrical double

layer (EDL), **2)** Helmholtz-Smoluchowski (HS) velocity ($U_{HS} = -\frac{E_x \varepsilon \zeta}{\mu c}$), which is proportional to external electric field (E_x), and **3)** Jefferys first parameter (ratio of relaxation time to retardation time (λ_1)). All other parameters i.e. $\varepsilon, \zeta, \mu, c$ are prescribed constant.

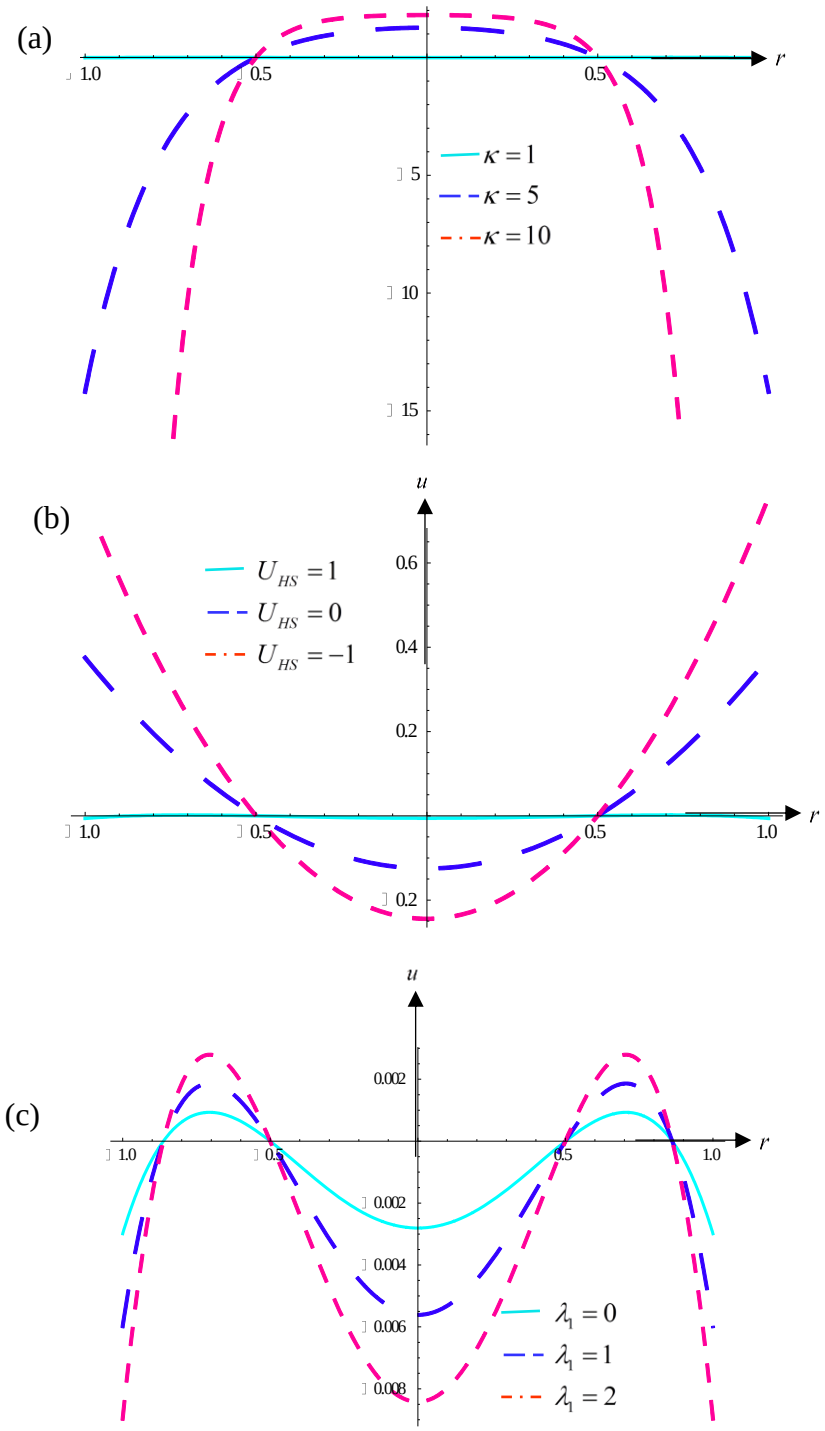

Fig.2. Velocity profile (axial velocity vs. radial coordinate) at $\phi = 0.5,$ and **(a)** $U_{HS} = 1, \lambda_1 = 1$ **(b)** $\kappa = 1$, $\lambda_1 = 1$ **(c)** $\kappa = 1$, $U_{HS} = 1$.

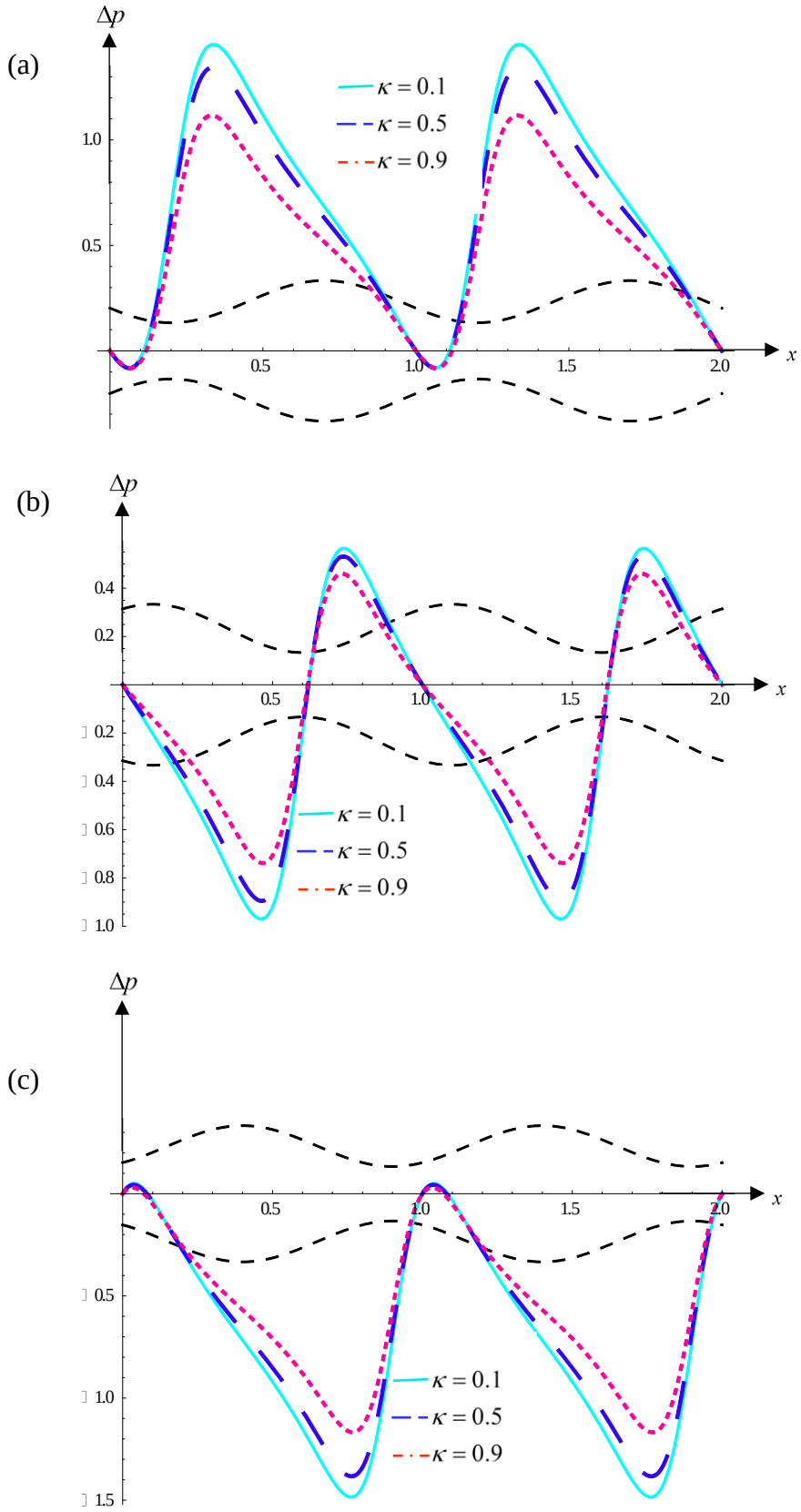

Fig.3. Pressure distribution along the length of tube at $\phi = 0.6, l = 2, U_{HS} = 1, \lambda_1 = 1$ at different time period (a) $t = 0.2$ (b) $t = 0.6$ (c) $t = 0.9$. Color lines represent the pressure distribution for different values of Debye length and Black dotted lines show the train wave propagation and single wave propagation.

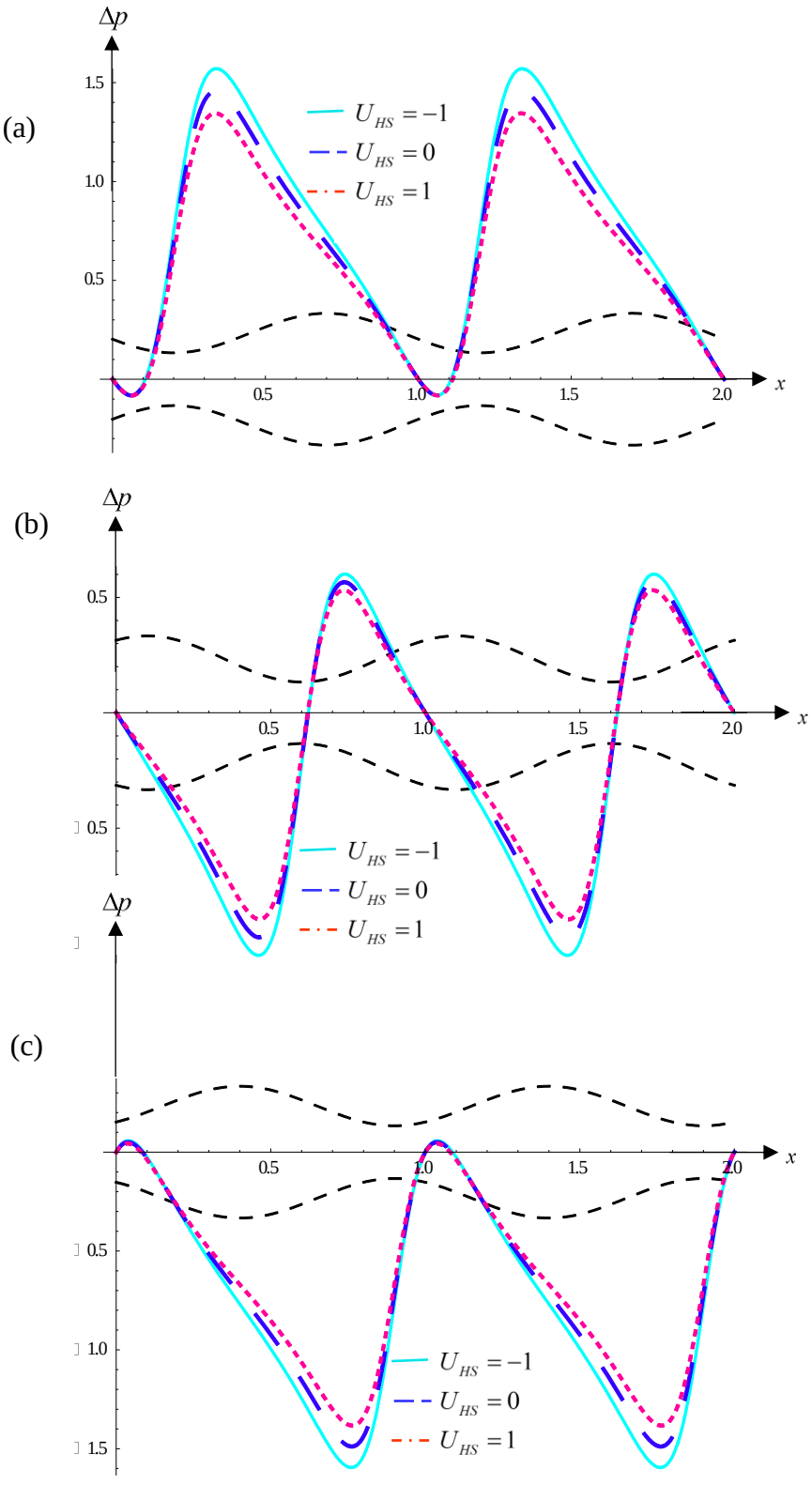

Fig.4. Pressure distribution along the length of tube at $\phi=0.6, l=2, \kappa=0.5, \lambda_1=2$ at different time period (a) $t=0.2$ (b) $t=0.6$ (c) $t=0.9$. Color lines represent the pressure distribution for different values of Helmholtz-Smoluchowski velocity and Black dotted lines show the train wave propagation and single wave propagation.

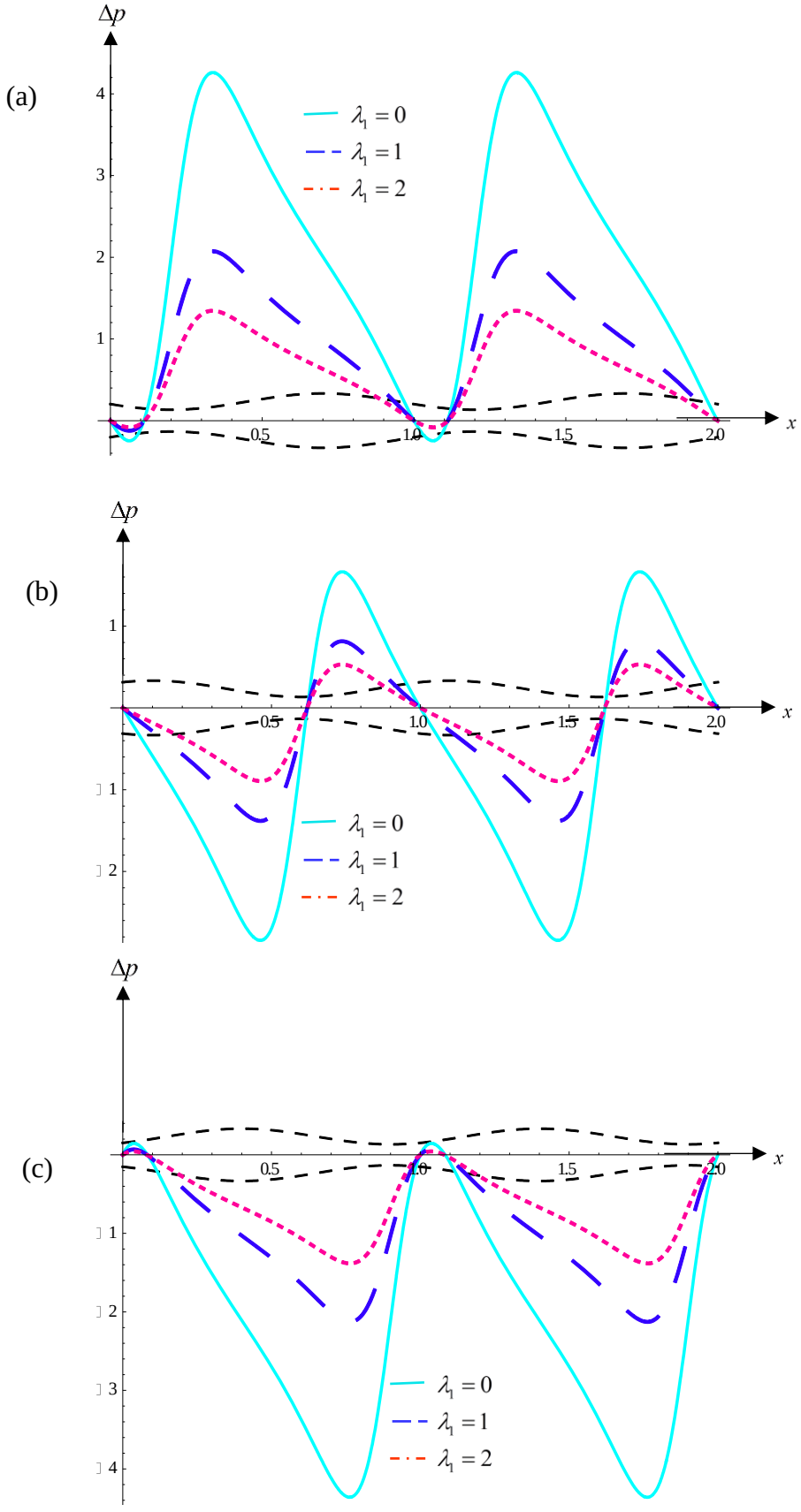

Fig.5. Pressure distribution along the length of tube at ϕ *=0.6, l=2,* κ *=0.5,* U_{HS} *=1* at different time period (a) $t = 0.2$ (b) $t = 0.6$ (c) $t = 0.9$. Color lines represent the pressure distribution for different

values of relaxation time and Black dotted lines show the train wave propagation and single wave propagation.

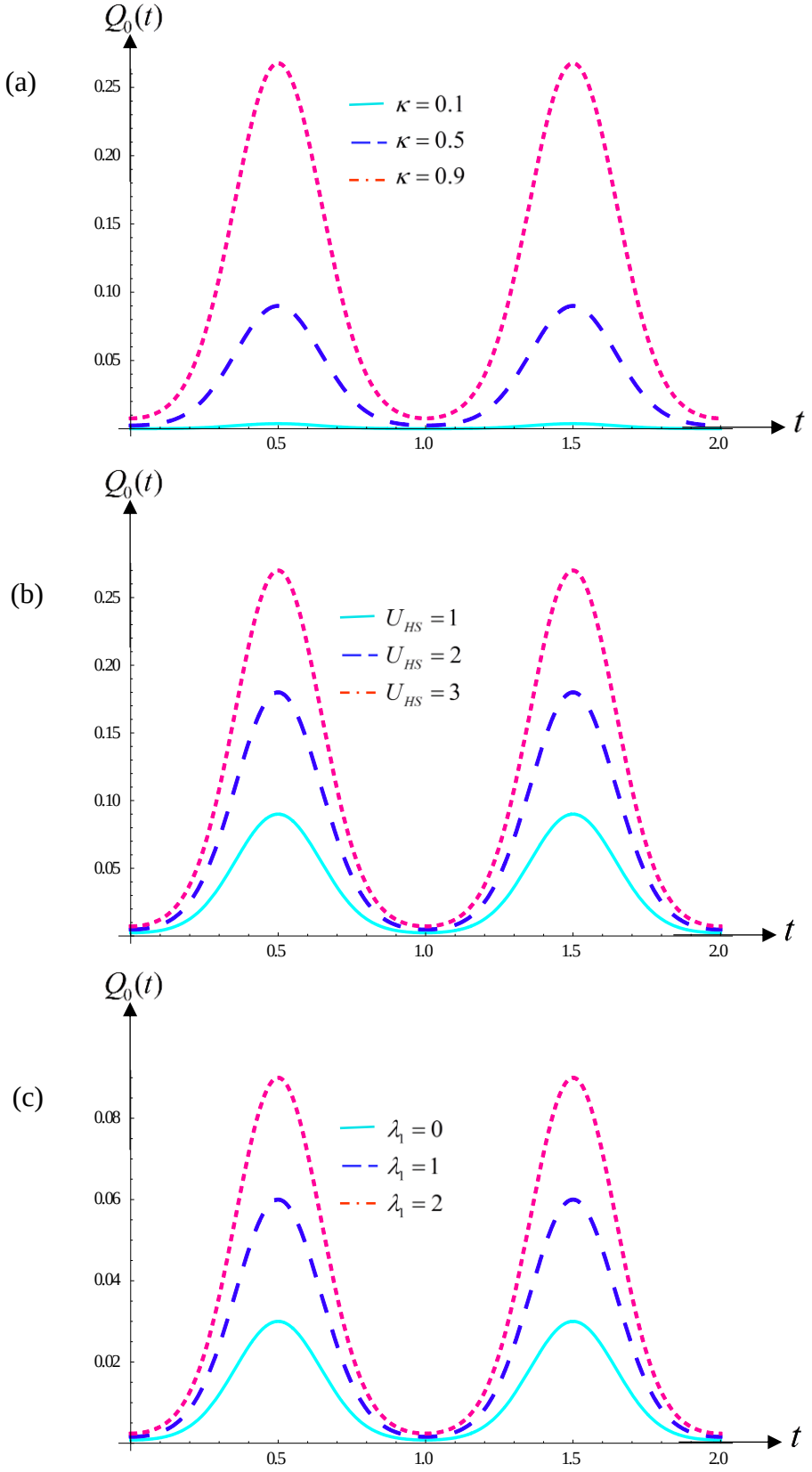

Fig.6. Maximum volumetric flow rate vs. time at $\phi = 0.6$, **(a)** $U_{HS} = 1, \lambda_1 = 2$ **(b)** $\kappa = 0.5$, $\lambda_1 = 2$ **(c)** $\kappa = 0.5$, $U_{HS} = 1$.

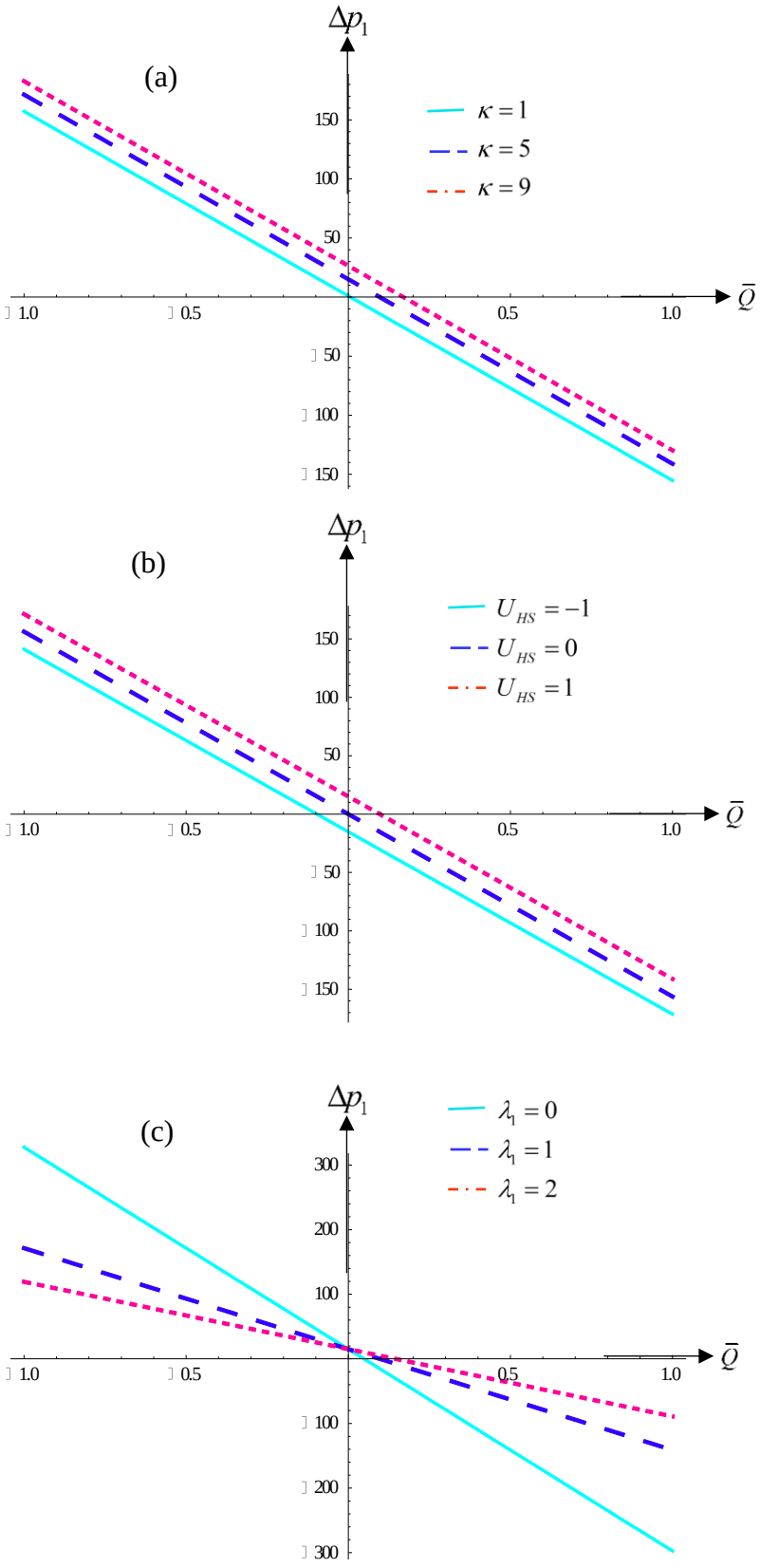

Fig.7. Pressure difference across one wavelength (Δp_1) vs. time averaged volumetric flow rate ($\bar{Q}$) for $\phi = 0.6$, **(a)** U_{HS} =1, $\lambda_1 = 1$ **(b)** κ =5, $\lambda_1 = 1$ **(c)** κ =5, U_{HS} =1.

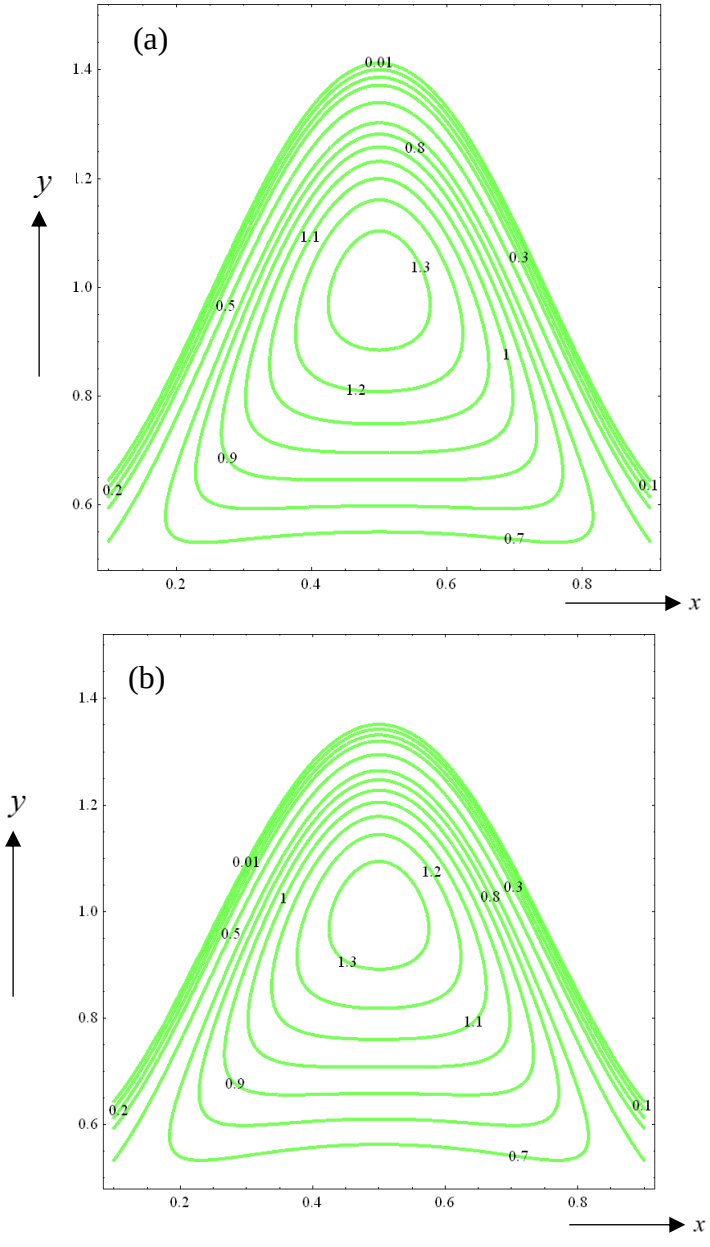
(a)
y
x
1.4
1.2
1.0
0.8
0.6
0.2
0.4
0.6
0.8
0.01
0.8
1.1
1.3
0.3
0.5
1
1.2
0.9
0.2
0.1
0.7
(b)
y
x
1.4
1.2
1.0
0.8
0.6
0.2
0.4
0.6
0.8
0.01
1.2
1
0.8
0.3
0.5
1.3
1.1
0.9
0.2
0.1
0.7

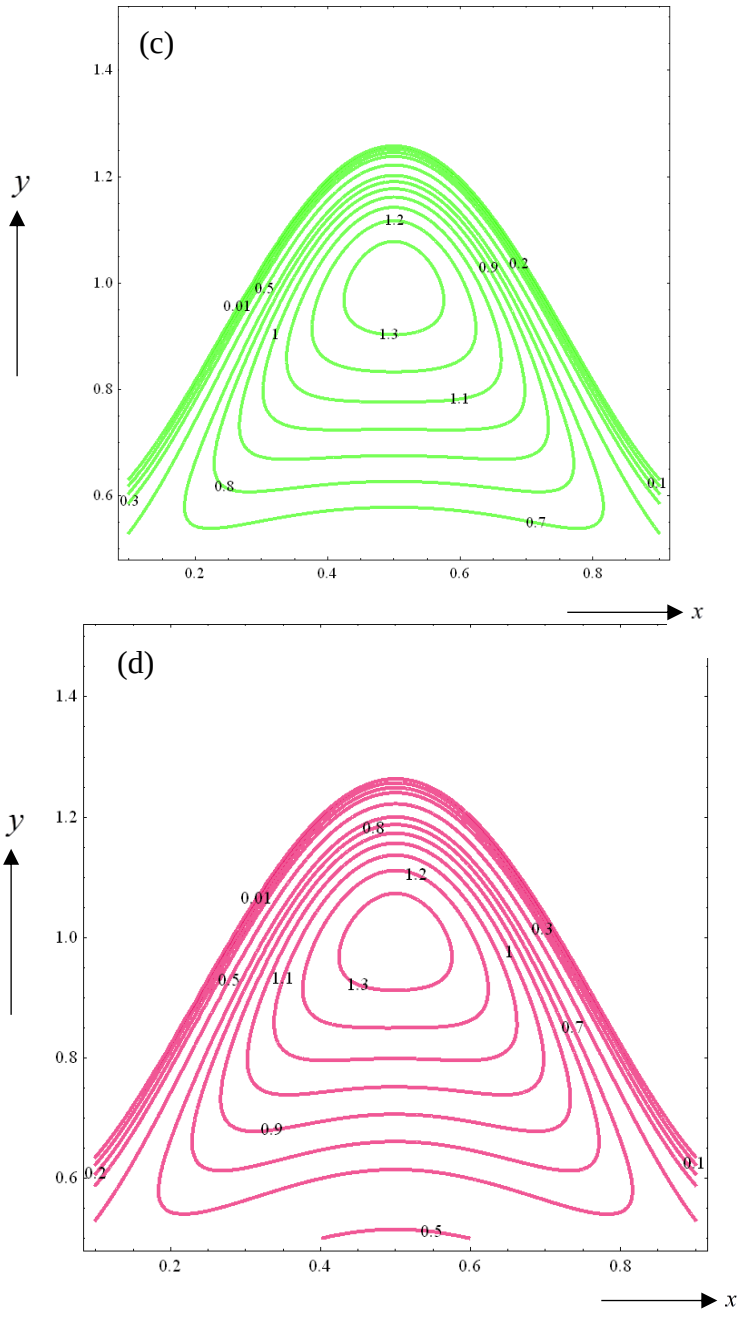
(c)
y
x
1.4
1.2
1.0
0.8
0.6
0.2
0.4
0.6
0.8
1.2
0.9
0.2
0.5
0.01
1
1.3
1.1
0.8
0.1
0.3
0.7
(d)
y
x
1.4
1.2
1.0
0.8
0.6
0.2
0.4
0.6
0.8
0.8
1.2
0.01
0.3
1
0.5
1.1
1.3
0.7
0.9
0.2
0.1
0.5

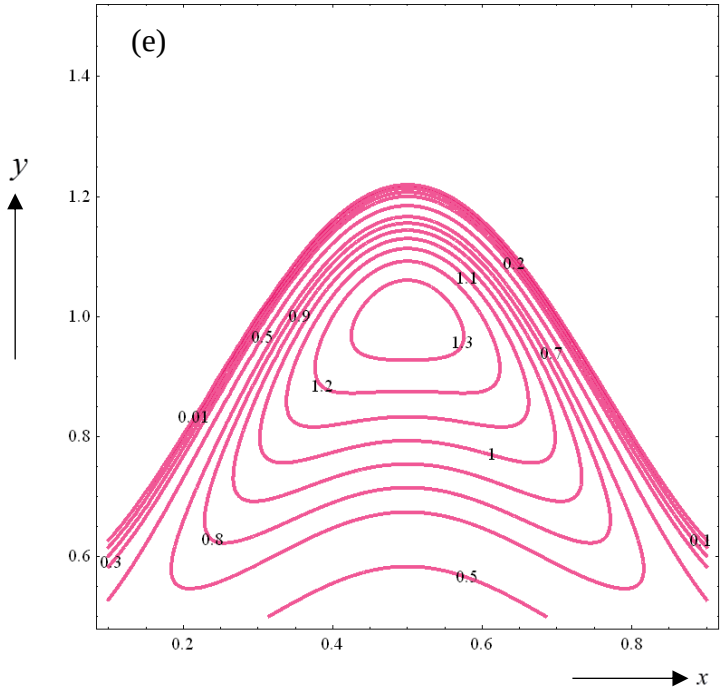
(e)
y
x
1.4
1.2
1.0
0.8
0.6
0.2
0.4
0.6
0.8
0.2
1.1
0.9
0.5
1.3
0.7
1.2
0.01
1
0.8
0.1
0.3
0.5

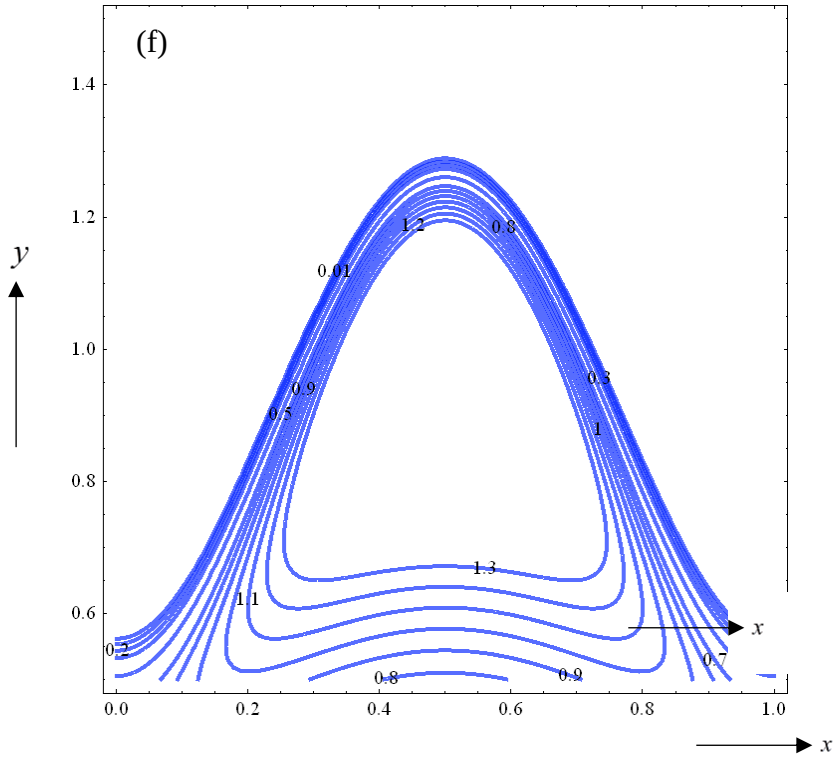
(f)
y
x
1.4
1.2
1.0
0.8
0.6
0.0
0.2
0.4
0.6
0.8
1.0
1.2
0.8
0.01
0.3
0.9
0.5
1
1.3
1.1
0.2
0.7
0.8
0.9

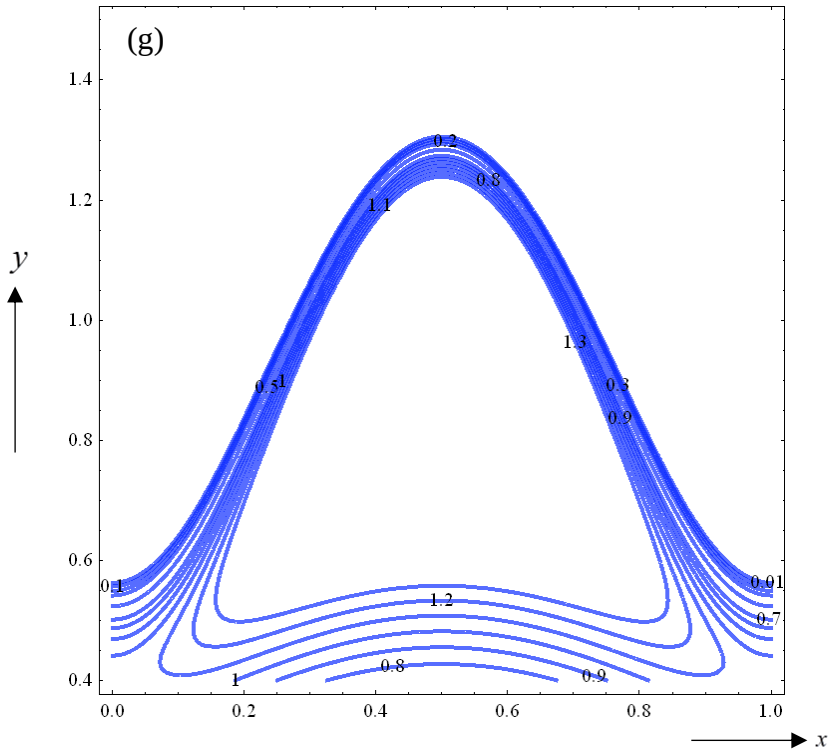

Fig.8. Stream lines in wave form at $\phi = 0.6, \bar{Q} = 0.9$ **(a)** κ *=1,* U_{HS} *=1,* λ_1*=1* **(b)** κ *=5,* U_{HS} *=1,* λ_1*=1* **(c)** κ *=10,* U_{HS} *=1,* λ_1*=1* **(d)** κ *= 5,* U_{HS} *=5,* λ_1*=1* **(e)** κ *=5,* U_{HS} *=10,* λ_1*=1* **(f)** κ *=5,* U_{HS} *=5,* λ_1*=2* **(g)** κ *=0.5,* U_{HS} *=1,* λ_1*=3.*

Fig. 2a shows that the axial velocity is enhanced with increasing electroosmotic parameter (κ) in the core region of the channel. Axial flow is however decelerated in the vicinity of the conduit wall significantly with greater κ values. The profiles evolve from strong inverted parabolas to plug-flow geometry with *increasing* electro-osmotic parameter. Debye length, λ_d , is *inversely related* to the electro-osmotic parameter, and quantifies the influence of a charge carrier's overall electrostatic effect in the viscoelastic electrolyte and therefore how deep into the bulk fluid these electrostatic effects are sustained. Increasing Debye length (decreasing electro-osmotic parameter) therefore decelerate the core flow and accelerate the near wall flow in the channel. We reiterate that in these figures ε (permittivity), ζ (zeta potential of the medium), μ (dynamic viscosity of viscoelastic electrolyte) and peristaltic wave velocity (c) are all fixed as is the wave amplitude (ϕ). With an increase in Helmholtz-Smoluchowski velocity ($U_{HS} = -\dfrac{E_x \varepsilon \zeta}{\mu c}$), i.e. a rise in axial external electric field strength, E_x the axial velocity in fig. 2b is observed to increase from negative values to zero (vanishing velocity) in the central zone

of the channel ($-0.5 \leq r \leq +0.5$). However with greater radial distance a significant decrease in axial velocity arises with greater Helmholtz-Smoluchowski (U_{HS}) values. Evidently therefore the influence of axial electrical field is dependent on the location in the conduit. Acceleration is only produced in the core region whereas deceleration is induced in the peripheral regions (at and close to the walls). The effect of increasing axial field on the peristaltic flow for $U_{HS} \leq 0$ is not consistent across the cross-section of the conduit. It is also interesting to note that for $U_{HS} = 1$ the velocity profile is linear across the channel i.e. axial velocity is invariant with radial coordinate. This implies that if a homogenous velocity profile is needed across the capillary or micro-scale device, the maximum electro-osmotic velocity of unity can achieve this result. Fig 2c demonstrates the influence of the Jefferys viscoelastic parameter ($\lambda_1=2$) on axial velocity profiles. An alternating response is computed. In the conduit core section $-0.5 \leq r \leq +0.5$, an increase in λ_1 generates significant retardation in the flow i.e. opposes axial momentum development. However external to this core, in the zones $-1.0 \leq r \leq -0.5$ and $0.5 \leq r \leq 1.0$, the axial flow is strongly accelerates, attains a peak and only very close to the conduit wall does the deceleration effect return. λ_1 relates the relaxation time to retardation time in the viscoelastic fluid. Yoo and Joseph [**46**] have shown that in viscoelastic fluid models including Jefferys model and the Maxwell model, with greater relaxation time, the fluid is more elastic and damping is suppressed near the boundaries. However in core flows the converse effect is induced and damping is accentuated which leads to deceleration in viscoelastic flows in the core zone of conduits. Similar observations have been reported by Haroun [**47**]. These trends concur with the present observations as illustrated in fig. 2c. Furthermore with $\lambda_1 = 0$ the Newtonian viscous case is retrieved and clearly in the core region Newtonian electro-osmotic flows are accelerated compared with viscoelastic flows. For $\lambda_1 = 1, 2$ the relaxation time is respectively equal to and double the retardation time. In general viscoelastic models, the retardation time of the material quantifies the time taken for the creep strain to accumulate; the shorter the retardation time, the more rapid the creep straining. It is therefore a very different phenomenon from stress relaxation which is related to time taken for bond rotations to take place and quantifies the time elapsed in relaxing to a new state (a measure of the time taken for the stress to relax; the shorter the relaxation time, the more rapid the stress relaxation). An advantage of the Jefferys model is that it possess both retardation and relaxation features, unlike for example the Maxwell model which cannot simulate a retarded elastic response or even the Voight model which does not address stress relaxation. Viscoelastic fluids behave as fully viscous fluids at one extremity and ideally elastic solids at the other. At the shear rates under consideration both viscous and elastic effects are of interest as are relaxation and retardation effects. Although biological materials exhibit an extensive

relaxation/retardation spectrum, the values of λ_1 =1, 2 employed in the current analysis are representative of actual viscoelastic electrolytes or gels both encountered in human physiology and in medical devices as described by Beebe *et al.* [**48**].

Figs. 3a-c illustrate the pressure difference (Δp) distributions along the axis of the conduit at different times (t) and with different electro-osmotic parameter values, κ. At low time values, there is a strong presence of positive pressure difference peaks along the channel extent. Simultaneously an increase in electro-osmotic parameter, κ (i.e. *decrease in electrical Debye length*) is found to *reduce* pressure differences in figs 3a and 3b (t =0.2 and 0.6 respectively) at the peaks but to enhance pressure difference at the troughs. With progressive time elapse the pressure differences are substantially reduced along the channel. For fig 3c, at t = 0.9, there is very little influence computed by altering the electro-osmotic parameter at the peaks, whereas at the troughs pressure difference is again found to be elevated with greater values of κ. However the plots exhibit mainly negative pressure difference at high time value and positive pressure difference at lower time values. In all three figures the relaxation and retardation times of the viscoelastic electrolyte are equivalent (λ_1 =1).

Figs. 4a-c illustrate the pressure difference (Δp) distributions along the axis of the conduit at different times (t) and with different values of Helmholtz-Smoluchowski (U_{HS}). With increasing U_{HS} values i.e. stronger axial electrical field, there is a marked reduction in the pressure differences along the conduit length. This behaviour is consistent for both troughs and peaks at t = 0.2. However at t = 0.6 the decrease in pressure differences is observed only to arise at the peaks and not the troughs. With subsequent progress in time, fig. 4c (t = 0.9) shows that increasing axial electrical field i.e. greater Helmholtz-Smoluchowski (U_{HS}) velocity values infact sustains an enhancing effect on the pressure difference for all values of axial coordinate. The impact of time is therefore critical in generating a modification in the impact of maximum electro-osmotic velocity i.e. Helmholtz-Smoluchowski (U_{HS}) on pressure difference evolution in the conduit, although generally negative values are computed at t = 0.9.

Figs. 5a-c illustrate the pressure difference (Δp) distributions along the axis of the conduit at different times (t) and with different values of viscoelasticity parameter (λ_1). A significant depression in pressure difference is observed with increasing λ_1.values. The Newtonian case (λ_1 = 0) achieves the greatest pressure difference magnitudes, at t = 0.2 (fig. 4a). Furthermore at this time state, the pressure differences are principally positive along the channel length. However with larger times (figs. 4b,c), pressure differences become increasingly negative. At intermediate time (t = 0.6) the pressure differences are again suppressed with greater values of viscoelasticity

parameter (at the peaks) and this effect is even more amplified at higher time values. Both time and viscoelasticity therefore substantially modify the pressure distributions in electro-osmotic pumping.

Figs. 6a-c illustrate the evolution in maximum transient volumetric flow rate ($Q_o(t)$) with time (t) and with different values of **a)** *electro-osmotic parameter* (i.e. $\kappa = aez\sqrt{\frac{2n_0}{\varepsilon K_B T}} = \frac{a}{\lambda_d}$), **b)** Helmholtz-Smoluchowski velocity ($U_{HS} = -\frac{E_x \varepsilon \zeta}{\mu c}$) and **c)** Jefferys first viscoelastic parameter (ratio of relaxation time to retardation time, λ_1). In all three plots well-dispersed periodic profiles are captured which illustrate clearly the sinusoidal nature of the peristaltic flow. Flow rates are observed to alternate with time i.e. attaining respective peaks then troughs. With an increase in κ, U_{HS} *and also* λ_1 there is a consistent enhancement in the volumetric flow rate at any value of time. Effectively therefore greater electro-osmotic effect (smaller Debye length), stronger axial field and stronger stress relaxation in the viscoelastic electrolyte results in boosting flow rates. Magnitudes of flow rates are modified (non-trivially increased) with a change in electro-osmotic parameter, κ (fig. 6a) and Helmholtz-Smoluchowski velocity (fig. 6b) than with a change in viscoelastic parameter (fig. 6c).

Figs. 7a-c illustrate the distributions of pressure difference across one wavelength vs time averaged volumetric flow rate for different values of the electro-osmotic parameter (κ), Helmholtz-Smoluchowski i.e. maximum electro-osmotic velocity (U_{HS}) and Jefferys first viscoelastic parameter (ratio of relaxation time to retardation time, λ_1)., respectively. These graphs provide an insight into the perspective of the response in pressure difference for both positive and negative time-averaged volumetric flow rates (Q) i.e. for the case where the pumping is aligned in the direction of axial electrical field (positive Q) and the opposite scenario in which the flow is opposite to axial field orientation i.e. x-axis (negative Q). In all cases an intermediate peristaltic wave amplitude is imposed i.e. ϕ = 0.2 in these plots. With an *increase* in electro-osmotic parameter, κ, as shown in fig. 7a, there is a *significant elevation* in the pressure difference for both Q <0 and Q >0. However positive pressure difference is only generally associated with negative flow rate and vice versa for positive flow rate. Overall a stronger electro-osmotic effect (weaker Debye length) impacts noticeably and tends to increase the pressure difference at any flow rate. Similarly fig. 7b shows that as the Helmholtz-Smoluchowski velocity increases (and therefore stronger axial electrical field acts on the system), pressure difference is again boosted, for both negative and positive flow rates. The

influence is again sustained irrespective of values of Q. Stronger axial electrical field is therefore assistive to the peristaltic propulsion in the conduit. Fig. 7c demonstrates that with greater Jefferys first viscoelastic parameter, the response in pressure difference with volumetric flow rate is significant deviated from that in figs 7a,b. For negative flow rates (Q <0) i.e. reversed flow an increase in stress relaxation relative to retardation in the viscoelastic electrolyte strongly depresses the pressure difference. This implies that stronger viscoelastic effect is inhibitive to pressure build up in the peristaltic regime in this range of flow rates. However for positive flow rate (Q>0), the opposite effect is induced and there is a growth in pressure difference with increasing viscoelastic parameter (i.e. decreasing retardation time).

Figs. 8a-g present streamline visualizations in the conduit for different various values of electro-osmotic parameter (κ), maximum electro-osmotic velocity (U_{HS}) and non-Newtonian couple stress parameter (α). Comparing fig. 8a-c, for which both U_{HS} and λ_1 are given fixed values of unity, and electro-osmotic parameter (κ) varies from 1 through 5 to 10, it is apparent that with greater electro-osmotic effect, the intensity of streamlines near the conduit wall is very slightly reduced and there is weaker circulation generated in this location. The dual bolus (trapping zone) structure is marginally distorted with greater electro-osmotic effect. Comparing fig. 8d and e, for which both κ and λ_1 are fixed at values of 5 and 1, respectively, and U_{HS} increases from 5 to 10, it is apparent that with an in*crease* in axial electrical field (to which U_{HS} is proportional) there results a slight growth in the dual bolus system and the streamlines near the boundaries are constricted. Finally figs. 6f and 6g reveal that as λ_1 is increased (with both κ and U_{HS} fixed at values of 5 and 5, respectively), there is a much more significant growth in the dual bolus magnitudes which diverge across the conduit section and cause a constriction in streamlines in the central zone.

4. CONCLUSIONS

A mathematical model has been developed for electro-osmotic driven peristaltic pumping of Jefferys viscoelastic electrolytes in a finite length conduit under the action of an axially imposed electrical field. The conservation equations have been non-dimensionalized and analytical solutions derived in terms of Bessel functions, for *axial velocity, volumetric flow rate, pressure difference and pressure gradient, stream function and time averaged volume flow rate.* The effects of electro-osmotic parameter (inverse Debye length), Helmholtz-Smoluchowski velocity and Jefferys viscoelastic relaxation/retardation parameter on peristaltic

pumping characteristics and trapping phenomena are evaluated numerically with the aid of Mathematica software. The finite length tube Newtonian model Li and Brasseur [**22**] is shown to be a special case of the present study. These principal findings from the present computations are:

- Axial velocity is increased with increasing electroosmotic parameter and Helmholtz-Smoluchowski velocity in the core region of the channel. Axial flow is however decelerated in the vicinity of the conduit wall significantly with greater electroosmotic parameter and Helmholtz-Smoluchowski velocity (i.e. stronger axial electrical field) values. In the conduit core region, greater viscoelastic parameters induce strong deceleration in the axial flow whereas the converse effect is computed closer to the conduit wall.
- Pressure difference is *decreased* with greater electro-osmotic parameter, larger time elapse, increasing Helmholtz-Smoluchowski velocity and also with greater viscoelasticity parameter, across the conduit length.
- Volumetric flow rate at any value of time is boosted with increasing electroosmotic parameter (smaller Debye length), Helmholtz-Smoluchowski velocity and viscoelasticity (relaxation/retardation) parameter.
- Pressure difference is enhanced with stronger electro-osmotic effect (weaker Debye length) and larger Helmholtz-Smoluchowski velocity (i.e. stronger axial electrical field) at any flow rate.
- With greater electro-osmotic effect and higher Helmholtz-Smoluchowski velocity there is a weak growth in the dual bolus structures. However a much more prominent growth is computed with increasing viscoelastic parameter.

The present study has considered the *Jefferys viscoelastic model*. Future investigations will consider alternate non-Newtonian models e.g. micropolar fluids [**49**].

ACKOWLEDGEMENTS

O. Anwar Bég wishes to express his gratitude to the late Professor Howard Brenner of Chemical Engineering, MIT, USA, for his guidance on electro-hydrodynamics and viscoelastic fluids which has aided immensely in the present work. The support of Mrs. Wendy Lancaster and Miss Janine Matley of Salford University, School of Computing, Science and Engineering, is also gratefully acknowledged. The authors are also grateful to the reviewers for their

informative comments which have served to clarify certain aspects of the current work and improved the manuscript.

REFERENCES

[1] R. Bashir, D. Akin, R. Gomez, H. Li, W.-J. Chang and A. Gupta, From bioMEMS to bionanotechnology: Integrated biochips for the detection of cells and microorganisms, *Proc. Mater. Res. Soc.*, 773 (2003) 911.

[2] S. Bhattacharya, J. S. Jang, L. J. Yang, D. Akin and R. Bashir, Biomems and nanotechnology-based approaches for rapid detection of biological entities, *J. Rapid Methods Autom. Microbiol.*, 15 (2007) 1.

[3] B. Bhushan, Nanotribology and nanomechanics of MEMS/NEMS and BioMEMS/ BioNEMS materials and devices, *J. Microelectron. Eng*.,84 (2007) 387-412.

[4] Y. Kang, C. Yang, X. Huang, Dynamic aspects of electro-osmotic flow in a cylindrical microcapillary, *Int. J. Engineering Science*, 40 (2002) 2203–2221.

[5] Y. Kang, C. Yang and X. Huang, Electroosmotic flow in a capillary annulus with high zeta potentials, *J. Colloid and Interface Science*, 253 (2002) 285–294.

[6] S. Devasenathipathy and J.G. Santiago, *Electrokinetic Flow Diagnostics, Micro- and Nano-Scale Diagnostic Techniques*, New York, Springer-Verlag (2002).

[7] A. R. Minerick, A. E. Ostafin, H-C. Chang, Electrokinetic transport of red blood cells in microcapillaries, *Electrophoresis*, 23 (2002) 2165–2173.

[8] A.J. Chung, Donn Kim and David Erickson, Electrokinetic microfluidic devices for rapid, low power drug delivery in autonomous microsystems, *Lab Chip*, 8 (2008) 330–338.

[9] S. Chakraborty, Analytical solutions of Nusselt number for thermally fully developed flow in microtubes under a combined action of electroosmotic forces and imposed pressure gradients, *Int. J. Heat and Mass Transfer* 49 (2006) 810–813.

[10] A. Sharma, S. Chakraborty, Semi-analytical solution of the extended Graetz problem for combined electroosmotically and pressure-driven microchannel flows with step-change in wall temperature, *Int. J. Heat and Mass Transfer* 51 (2008) 4875–4885.

[11] R. Dey, D. Chakraborty, S. Chakraborty, Extended Graetz problem for combined electroosmotic and pressure-driven flows in narrow confinements with thick electric double layers, *Int. J. Heat and Mass Transfer* 55 (2012) 4724–4733.

[12] M. Mohammadi, H. Madadi, J. Casals-Terré, Jordi Sellarès, Hydrodynamic and direct-current insulator-based dielectrophoresis (H-DC-iDEP) microfluidic blood plasma separation, *Anal. Bioanal. Chem.* 407 (2015) 4733–4744.

[13] Sinha, A., and G. C. Shit. "Electromagnetohydrodynamic flow of blood and heat transfer in a capillary with thermal radiation." Journal of Magnetism and Magnetic Materials 378 (2015): 143-151.

[14] W**.** G. Paterson**,** Esophageal peristalsis, *GI Motility online* (2006) doi:10.1038/gimo13

[15] Y.C. Fung, *Biomechanics: Motion, Flow, Stress and Growth*, Springer, New York (1990).

[16] E. N. Kanu, K. A. Daltorio, R. D. Quinn and Hillel J. Chiel, Correlating kinetics and kinematics of earthworm peristaltic locomotion, *Biomimetic and Biohybrid Systems, Volume 9222, Lecture Notes in Computer Science* (2015) 92-96.

[17] V. Baran, Peristaltic locomotion in earthworms and adaptivity to next generation crawler robots for geological exploration, *MEng Thesis, Mechanical Engineering, Sheffield Hallam University, Dept. Engineering and Mathematics, Sheffield, UK, June* (2010).

[189] Megan Snowdon, Peristaltic hydrodynamics and trans-location modelling in botanical engineering, *MEng Thesis, Mechanical Engineering, Sheffield Hallam University, Dept. Engineering and Mathematics, Sheffield, UK, June* (2011).

[19] J. A. Milburn, Pressure Flow, *Transport in Plants I, Volume 1 of Encyclopedia of Plant Physiology* (1975) 328-353.

[20] J. A. Paré, An overview of pentastomiasis in reptiles and other vertebrates, *J. Exotic Pet Medicine*, 17 (2008) 285–294.

[21] A. H. Shapiro, M. Y. Jaffrin and S. L. Weinberg, Peristaltic pumping with long wavelengths at low Reynolds number, *J. Fluid Mech.* 37 (1969) 799-825.

[22] M. Li and J. G. Brasseur, Non-steady peristaltic transport in finite-length tubes, *J. Fluid Mech*., 248 (1993) 129-151.

[23] J. G. Brasseur and W. J. Dodds, Interpretation of intraluminal manometric measurements in terms of swallowing mechanics, *Dysphagia*, 6 (1991) 100-119.

[24] H.L. Goldsmith, Biorheology in the 21st century, *Biorheology*, 49 (2012) 103-108.

[25] J. de Vicente (Editor), *Viscoelasticity - From Theory to Biological Applications*, InTech, USA (2012).

[26] D. R. Picout and S. B. Ross-Murphy, Rheology of biopolymer solutions and gels, *The Scientific World J.* 3 (2003) 105–121.

[27] M. K. Chaube, D. Tripathi, O. Anwar Bég, Shashi Sharma and V.S. Pandey, Peristaltic creeping flow of power law physiological fluids through a non-uniform channel with slip effect, *Applied Bionics and Biomechanics* (2015). Volume 2015, Article ID 152802, 10 pages. http://dx.doi.org/10.1155/2015/152802

[28] N. Ali, M. Sajid, Z. Abbas, T. Javed, NonNewtonian fluid flow induced by peristaltic waves in a curved channel, *Eur. J. Mech.-B: Fluids*, 29 (2010) 387–394.

[29] D. Tripathi and O. Anwar Bég, Mathematica numerical simulation of peristaltic biophysical transport of a fractional viscoelastic fluid through an inclined cylindrical tube, *Computer Methods in Biomechanics and Biomedical Engineering*, 18 (2014) 1-10.

[30] G. Ravi Kiran, G. Radhakrishnamacharya and O. Anwar Bég, Peristaltic flow and hydrodynamic dispersion of a reactive micropolar fluid: simulation of chemical effects in the digestive process, *J. Mechanics in Medicine and Biology (2016). DOI: 10.1142/S0219519417500130 (17 Pages)*

[31] D. Tripathi, and O. Anwar Bég, Transient magneto-peristaltic flow of couple stress biofluids: a magneto-hydro-dynamical study on digestive transport phenomena, *Mathematical Biosciences,* 246 (2013) 72-83.

[32] M. Kothandapani, J. Prakash, Effects of thermal radiation parameter and magnetic field on the peristaltic motion of Williamson nanofluids in a tapered asymmetric channel, *Int. J. Heat and Mass Transfer* 81 (2015) 234–245.

[33] L. Giraud, D. d'Humières and P. Lallemand, A lattice Boltzmann model for Jeffreys viscoelastic fluid, *Europhysics Lett.,* 42 (1998) 625-630.

[34] S.Abdul Gaffar, V.R. Prasad and O. Anwar Bég, Flow and heat transfer of Jefferys non-Newtonian fluid from a horizontal circular cylinder, *AIAA J. Thermophysics and Heat Transfer,* 28 (2014) 764-770.

[35] A.F. Khadrawi, M.A. Al-Nimr, Ali Othman, Basic viscoelastic fluid flow problems using the Jeffreys model, *Chemical Engineering Science*, 60 (2005) 7131–7136.

[36] N. S. Akbar, S. Nadeem and M. Ali, Jeffrey fluid model for blood flow through a tapered artery with a stenosis, *J. Mech. Med. Biol.* 11 (2011) 529-539.

[37] T. Alarabi, A. F. Elsayed and O Anwar Bég, Homotopy perturbation method for heat transfer in peristaltic flow of viscoelastic fluid in an eccentric cylinder with variable effects, *Life Science Journal,* 11 (2014) 197-206.

[38] D. Tripathi, S.K. Pandey and O. Anwar Bég, Mathematical modelling of heat transfer effects on swallowing dynamics of viscoelastic food bolus through the human oesophagus, *Int. J. Thermal Sciences*, 70 (2013) 41–53.

[39] S. Chakraborty, Augmentation of peristaltic microflows through electro-osmotic mechanisms, *J. Phys. D: Appl. Phys.* 39 (2006) 5356–5363.

[40] C. Zhao, E. Zholkovskij, J. H. Masliyah, C. Yang, Analysis of electroosmotic flow of power-law fluids in a slit microchannel, *J. Colloid and Interface Science*, 326 (2008) 503–510.

[41] P. M. Coelho, M. A. Alves, F. T. Pinho, Forced convection in electro-osmotic/Poiseuille micro-channel flows of viscoelastic fluids: fully developed flow with imposed wall heat flux, *Microfluidics and Nanofluidics*, 12 (2012) 431-449.

[42]C. O. Ng and C. Qi, Electro-osmotic flow of a viscoplastic material through a slit channel with walls of arbitrary zeta potential, *Physics of Fluids*, 25 (2013) 3102-3108.

[43] N. A Mishchuk, A. V. Delgado, S. Ahualli and F. González-Caballero, Nonstationary electro-osmotic flow in closed cylindrical capillaries. Theory and experiment, *J. Colloid and Interface Science,* 309 (2007) 308-14.

[44] P. H. Paul, M. G. Garguilo, and D. J. Rakestraw, Imaging of pressure- and electrokinetically driven flows through open capillaries, *Anal. Chem*. 70 (1998) 2459-2467.

[45] J-H. Chang, S-F. Cheng, The operation characteristics and electrochemical reactions of a specific circulation-enhanced electrokinetics**,** *J. Hazardous Materials*, 141 (2007) 168-175.

[46] J.Y. Yoo and D.D. Joseph, Hyperbolicity and change of type in the flow of viscoelastic fluids through channels, *J. Non-Newtonian Fluid Mechanics*, 19 (1985) 15-41.

[47] M. H. Haroun, Effect of relaxation and retardation time on peristaltic transport of the Oldroydian viscoelastic fluid, *J. Applied Mechanics and Technical Physics*, 46 (2005) 842–850.

[48] D.J. Beebe *et al.*, Functional hydrogel structures for autonomous flow control inside microfluidic channels. *Nature*, 404 (2000) 588-590.

[49] A.A. Siddiqui and A. Lakhtakia, Steady electro–osmotic flow of a micropolar fluid in a microchannel, *Proc. Roy. Soc. London A*, 465, 2009, 501 – 522.